ACS APPLIED MATERIALS & INTERFACES

Research Article

www.acsami.org

Characterization of the Microstructure of GaP Films Grown on {111} Si by Liquid Phase Epitaxy

Susan R. Huang,*[,†,‡] Xuesong Lu,[§,⊥] Allen Barnett,[§,#] Robert L. Opila,*[,†] Vishnu Mogili,[∥,□] David A. Tanner,[∥,□] and Shohei Nakahara[∥,○]

[†]Department of Materials Science and Engineering, 201 DuPont Hall, University of Delaware, Newark, Delaware 19716, United States

[§]Department of Electrical and Computer Engineering, 140 Evans Hall, University of Delaware, Newark, Delaware 19716, United States

[∥]Materials & Surface Science Institute, [□]Department of Design & Manufacturing Technology, and [○]Department of Physics & Energy, University of Limerick, Limerick, Ireland

ABSTRACT: The development of a cost-effective Si based platform on which III−V's can be grown is of great interest. This work investigates the morphology of gallium phosphide (GaP) films grown on {111} silicon (Si) substrates by means of liquid phase epitaxy in a tin (Sn) - based solvent bath. Two types of single-crystal {111} Si substrates were used; the first type was oriented exactly along the ⟨111⟩ surface (no-miscut) and the second was miscut by 4°. The growth rate of the GaP films was found to be markedly different for the two types of substrates; the GaP films on the miscut Si substrate grew ∼4 times faster than those on the no-miscut substrate. The GaP films grew epitaxially on both types of substrates, but contained Si and Sn as inclusions. In the case of the no-miscut substrate, a number of large Sn particles were incorporated at the GaP/Si interface. As a result, these interfacial Sn particles affected the strain state of the GaP films dramatically, which, in turn, manifested itself in the form of a duplex microstructure that consists of strained and strain-free regions.

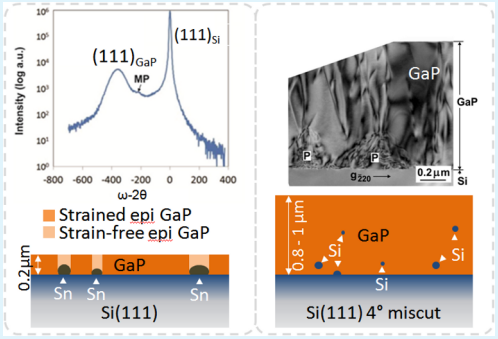

KEYWORDS: *III−V compound semiconductor materials, XRD, (S)TEM, liquid phase epitaxy*

1. INTRODUCTION

The ability to grow III−V semiconductors on a silicon substrate is of keen interest to the semiconductor device community as it opens the possibility of integrating the electronic performance of III−V semiconductors while taking advantage of highly developed and cost-efficient silicon substrates. One particular application for a Si-based platform on which III−V materials can be grown is the series connected multijunction solar cell which generally employ Ge or III−V substrates. However, the cost advantages of developing the cell stack on a Si-based substrate could open the door for multijunction cells to reach a broader range of applications, such low concentration and simpler tracking configurations. Gallium phosphide (GaP) is one of the III−V compound semiconductors that has a low lattice mismatch to silicon (Si); the amount of the mismatch between GaP and Si is 0.38%, which is within the acceptable range for epitaxial growth in this class of materials[1] and holds promise for the development of a Si-based platform for III−V growth. Epitaxial growth of GaP on Si has been previously explored for the possible integration of optoelectronic devices on mature Si platforms, using various growth methods, such as halide transport,[2] metalorganic vapor phase epitaxy,[3] chemical beam epitaxy,[4] molecular beam epitaxy,[5] and their combinations.[6] Recently, MOCVD growths of GaP performed on Si(100) have exhibited island growth,[7] although processes for obtaining planar growth with low TDD interfaces have been achieved on Si(100) faces through careful engineering of the substrate miscut and use of a silicon pre-epitaxial step.[8]

Although previous studies covered the physical and device characteristics of GaP/Si structures grown by the above methods extensively, very little work on GaP/Si systems obtained by liquid phase epitaxy (LPE) has been reported.[9,10] In contrast to other growth techniques, the main advantage of an LPE growth method lies in the fact that it can be carried out in near-equilibrium conditions and at low temperatures if an appropriate liquid metal is chosen for the bath solvent. LPE is currently widely used in industry for growth of light-emitting diodes[11] and is a promising growth method for devices that do not require nanometer scale features such as photovoltaics.

The present project was undertaken to understand the microstructure of LPE GaP films grown on {111} Si substrates in a tin - based solvent bath. In addition, the effect of the substrate miscut on the microstructure was studied by choosing two types of Si substrates; one has the exact {111} surface and

Received: June 8, 2014
Accepted: October 9, 2014
Published: October 9, 2014

the other miscut by 4°. Epitaxial films were achieved and the strain state and chemical composition were characterized using AFM, SEM, XPS, XRD, and TEM. It is shown that incorporation of Sn particles occurs at the GaP/Si interface and has a dramatic effect on the microstructure.

2. EXPERIMENTAL PROCEDURE

LPE GaP films were grown on Si substrates in a horizontal quartz reactor tube with a sliding three-zone furnace. High-purity graphite boats were made to hold the growth solutions, in which 99.99%-pure Sn was chosen as the bath solvent. The Sn solvent has an advantage of offering a high GaP-to-Si solubility ratio[12] and, at the same time, Sn acts as an n-type dopant in GaP without introducing deep recombination centers. Polycrystalline GaP pieces (99.999% purity) were used as the solute at 2.5 mol % with respect to the amount of Sn. A low percentage (0.5 at %) of magnesium was added as a reducing agent to remove residual or regrown oxide on the seed substrate during growth. Since the Sn solution wets the Si wafer poorly,[13] 5 at % bismuth was added to help promote wetting[14] and thus to achieve uniform growth layer coverage.

Growth of GaP films was initially attempted on the {100} Si surface. On this surface, however, only three-dimensional island growth resulted. These islands consisted of various sizes of square-base pyramids having the 4 {111} faces with the basal edges running along the ⟨110⟩ directions. Therefore, {111}-oriented substrates were used rather than the {100} Si substrates.

Two types of boron-doped (1×10^{15} cm^{-3}) and 380 μm thick {111} Si wafers were used as the substrates; the wafer surface of the first type had a perfect {111} face within an alignment of ±0.4°, whereas that of the second type had a 4°-miscut surface, which was miscut toward one of the three ⟨110⟩ directions of the surface. Hereafter, these two types of substrates are referred to as no-miscut and miscut substrates. Importantly, it was necessary to add Si into the solvent bath to prevent dissolution of the seed substrate in the bath. Therefore, a sacrificial phosphorus-doped (n-type) Si wafer was used to saturate the bath solution with Si at the initial growth temperature. Before the growth, all the Si substrates were cleaned using the standard Si cleaning processes, which remove oxides as well as ionic/organic surface impurity residues.

Immediately before being introduced into the growth chamber, the substrates were etched in a dilute hydrofluoric solution to remove any surface oxide, which is a known impediment to epitaxial growth.[15] To reduce the chances of oxidation during GaP growth, the chamber was pumped down to 50 mTorr, followed by triple purging with 99.999% pure argon gas, and then was finally flooded with an ultrapure (99.99998%) hydrogen flow at a rate of 300 cc/min from a hydrogen generator. The growth chamber was first heated to 910 °C to homogenize the solvent solution and to reduce the occurrence of step bunching on the substrate surface,[16] followed by cooling to 750 °C, at which point the solution was moved over the sacrificial n-type Si wafer for 30 min. The solution was then removed from the sacrificial Si and cooled to 748 °C to create a supersaturated state for the purpose of promoting the subsequent GaP nucleation processes. Finally, the Si seed substrate was brought in contact with the Si-supersaturated solution. The growth of GaP films took place at a cooling rate of 0.3 °C/min and for the total temperature difference of 30 °C, at the end of which the solution was separated from the substrate, and the system was allowed to cool to room temperature.

A scanning electron microscope (SEM) and an atomic force microscope (AFM, Pacific Nanotechnology) in the tapping mode were used to characterize the surface morphology of the GaP epitaxial films. A JEOL JSM-7400f SEM equipped with an energy dispersive X-ray (EDX) spectrometer with a lateral resolution of 2 nm and an acceleration voltage of 10 kV was used for imagining and composition analysis.

For the determination of the chemical composition in the near-surface region (0−10 nm in depth) of the GaP films, X-ray photoelectron spectroscopy (XPS) was performed using a 20−500 μm focused-beam of monochromatic aluminum $K\alpha$ X-rays. To generate atomic percentage values, we corrected each raw XPS signal by dividing its signal intensity (the number of electrons detected) by a "relative sensitivity factor", and normalized it over all of the elements detected.

High-resolution X-ray diffraction (HRXRD) triple-axes measurements were done using a Phillips X'Pert-MRD equipped with a 4-bounce (220) Ge monochromator at the source. A 3-bounce (220) Ge analyzer crystal in front of the detector provided the third axis and limited the acceptance angle of the detector to 12 arcseconds. For the measurements of the lattice mismatch and strain state for the GaP films, both $\omega-2\theta$ and ω (rocking curve) scans were taken around the (111) Si reflection with reflecting planes parallel to the substrate surface.

The transmission-electron-microscope (TEM) specimens were prepared by the standard method that includes several steps, such as cleaving, sandwiching, mechanical polishing, and final ion-milling using a precision ion polishing system (PIPS) from Gatan. TEM examinations were carried out using a JEM 2100 field-emission electron microscope equipped with an EDX spectrometer. In addition to the conventional bright- (BF) and dark-field (DF) imaging, an imaging technique called, "high-angle annular dark field (HAADF)" imaging was applied in the scanning mode (STEM) to obtain a variation in the dark-field image contrast that is sensitive to the type of atomic species; the higher the atomic number, the brighter the contrast.

To understand the atomic composition of inclusions observed in the GaP films, we used a chemical etching method, which was previously employed to identify iron phosphide particles in indium phosphide[17] and Si particles in SiO_2 matrix.[18] In the present experiment, a 5% Br-methanol solution was used as an etchant for the GaP film. A few drops of the etching solution were applied on the surface of the GaP film. After the GaP film is preferentially etched away, the remaining etching solution as well as unetched inclusions left on the Si substrate was air-dried overnight. The air-drying left a residue on the substrate. This surface residue was first analyzed by SEM/EDX and then collected on a carbon-coated copper grid for subsequent TEM/EDX examinations as described previously.

3. RESULTS AND DISCUSSION

3.1. Growth Rate. One of the interesting results was that the growth rate of the GaP films was markedly different for the two types of substrates; the growth rate of the GaP films grown on the miscut Si substrate was ∼4 times faster than those on the no-miscut substrate. This result is understandable from the fact that the miscut substrate contains a certain number of geometrically necessary surface steps, which can promote the growth of the GaP through increased step-flow mode growth events. The no-miscut surface, on the other hand, does not have such steps, which necessitates a Stranski-Krastanov or Volmer−Weber type growth. Thus, the difference in the growth rate between the two GaP films can be attributed to the density of steps between the two substrates.

3.2. Surface Morphology. The surface morphology of the GaP films was studied using SEM and AFM. Images a and b in Figure 1 show the surface of thin (∼70 nm) and thick (∼200 nm) GaP films grown on the no-miscut substrates. The surface of the thin deposit is smooth, but it is covered with particles (marked with white triangles) (see Figure 1a) that are likely due to residual Sn solvent trapped on the surface after the Sn bath is separated from the substrate. These particles, however, are not present on the thicker film (cf. Figure 1b). For the thick film, the surface was flat with occasional large (60−70 μm in diameter) circular plateaus (marked with a symbol, S). According to AFM examinations, the edge of the plateau had a step height of ∼10 nm (see Figure 1c). A careful examination of the surface has revealed that some plateaus contained a spiral

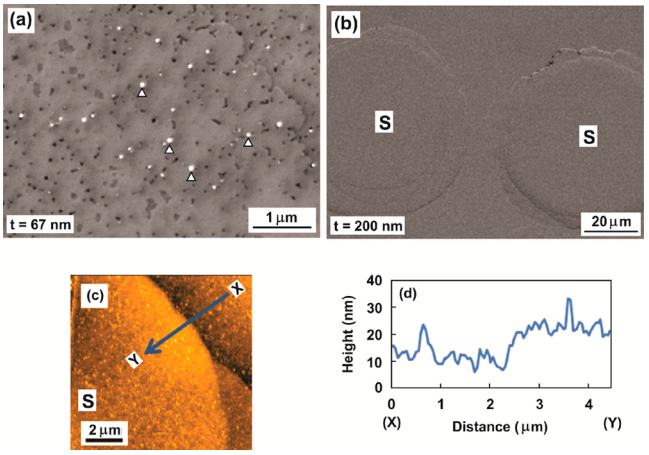

Figure 1. SEM and AFM micrographs showing the surface morphology of GaP films grown on the no-miscut {111} Si substrates. A number of round particles (marked with white triangles) are present on the surface of (a) the thin (67 nm) film but not present on (b) the thicker (200 nm) film. Large circular plateau is indicated with a symbol, S. In (c), an AFM image for the edge area of one of the plateaus (marked with a symbol, S) is shown together with (d) an X–Y line scan, which measures the average height of the plateau to be ∼10 nm.

step in the middle. This spiral growth form must have been mediated by screw dislocations emerging at the surface.

Images a and b in Figure 2 are SEM images showing the surface of 400 and 800 nm thick GaP films grown on the 4° miscut substrates. For the thinner film (cf. Figure 2a), the surface consists of a number of multiatomic steps. The main characteristic of these steps is that they are not a straight line but contain many jogs. The general direction of the step propagation is marked with a black arrow and is seen to run toward the ⟨110⟩ direction as expected. A careful examination of these steps indicates that a high density of large (up to 200 nm) round particles (seen as a bright spot) is adsorbed at the edge of these steps. These particles appear to have contributed to the inhibition of the step propagation, thus making a jog in the step edge. The surface of the thick film (cf. Figure 2b), on the other hand, does not show the image of steps directly, but its morphology resembles the step structure seen on the thin film (Figure 2a). Thus, the surface is not smooth and the average roughness is found to be ∼20 nm according to AFM measurements.

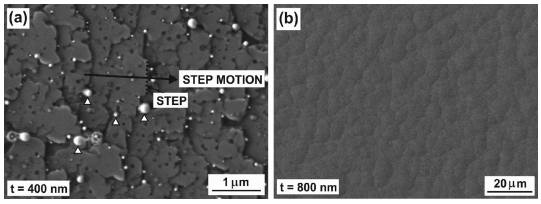

Figure 2. SEM micrographs showing the surface morphology of GaP films grown on the miscut {111} Si substrates. A number of round particles (marked with white triangles) are present on the surface of the thin (t = 400 nm) film, but not on that of the thicker (t = 800 nm) film. The direction of the step motion is indicated with a black arrow.

The bright particles seen in Figures 1a and 2a are most likely Sn and/or SnO, formed from liquid Sn left behind on the surface when the film/substrate was removed from the solvent bath at the end of growth. Because these particles are not present on the surface of thicker films (cf. Figure 1b and 2b), their presence must be related to the surface roughness associated with this particular thin films. These particles are particularly conspicuous for the miscut substrate (Figure 2a), because the surface is very rough at this range of thickness.

3.2. Composition of GaP Films by EDX. An qualitative estimate of the composition of the 200 nm thick GaP film grown on the no-miscut substrate as measured by EDX showed approximately 30% Ga–44% P–26% Si (in at %) in the plateau area (marked with a symbol, S) and 12% Ga–20% P–68% Si in the areas outside of the plateaus (see Figure 1b). The difference in the Si content between the two areas is attributable to a difference in the thickness of the GaP film. In other words, a Si signal from the underlying Si substrate may have contributed more to the thinner area, i.e. the area outside the plateau. The 800 nm GaP film grown on the miscut substrates, on the other hand, is less affected by the substrate due to the large thickness and indeed showed the composition of approximately 32% Ga–53% P – 15% Si consistently. It is important to note that regardless of the type of substrates used, both films appear to contain a large amount of Si.

3.4. Composition of GaP Films by XPS. The GaP films were also examined using XPS, which allows us to determine the composition of near the surface region within a depth of 10 nm. This allows for a measurement of the composition without an overestimate of the Si due to contribution from the substrate, as is the case with measurements performed using EDX. The XPS of Ga, P and Si from the 200 nm thick GaP film

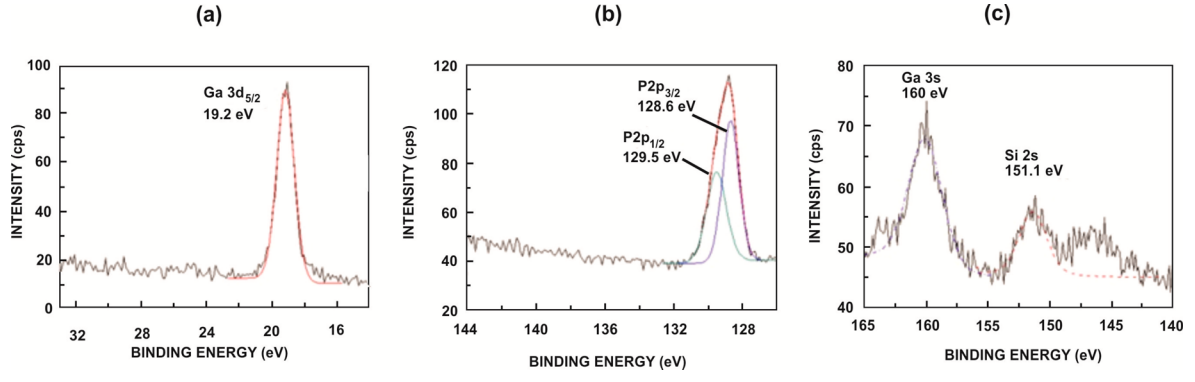

Figure 3. XPS spectra obtained from the surface of a 200 nm thick GaP layer grown on the no-miscut {111} Si substrate. Three ranges of binding-energy, which contain (a) the Ga $3d_{3/2}$, (b) P 2p, and (c) Si 2s peaks, are plotted.

dx.doi.org/10.1021/am503448g | ACS Appl. Mater. Interfaces 2014, 6, 18626–18634

grown on the no-miscut substrate are shown in Figure 3. In panels a and b in Figure 3, the peaks for Ga $3d_{5/2}$ and P $2p_{3/2}$ are centered at 19.2 eV and 128.6 eV, respectively. Both peaks are consistent with the binding energies of GaP.[19]

The widely used Si 2p peak at a binding energy of around 100 eV was initially selected but it is located approximately at the same energy as the Ga $3p_{3/2}$ peak. Thus, it was difficult to deconvolute these two peaks of Ga and Si from the spectrum in this energy range. To avoid these overlapped peaks, we selected the Si 2s peak instead. The Si 2s peak of the film is located at 151.1 eV, which corresponds to the Si^{2+} oxidation state. The Ga 3s peak in this region is 10 eV higher in binding energy than the Si 2s peak (Figure 3c). The atomic concentration, as estimated by instrumental sensitivity factors, is approximately 44% Ga, 42% P and 14% Si. This composition further confirmed that GaP was produced by LPE with additional Si incorporation beyond the equilibrium concentration in the film, which is consistent with the EDX measurements.

3.5. Crystallinity and strain State Determined by HRXRD $\omega-2\theta$ and ω Rocking Curves. An HRXRD analysis was made to measure the crystal quality, the degree of relaxation resulting from coherency breakdown, and the dislocation density in the GaP films. All films examined were thicker than the approximation of the critical thickness based on lattice mismatch for GaP and Si, which is around 13 nm. For this analysis, both $\omega-2\theta$ and ω rocking curves were taken around the {111} GaP reflection with reflecting planes parallel to the substrate surface. As noted in the $\omega-2\theta$ curve in panels a and c in Figure 4, the GaP films are crystalline and exhibits the

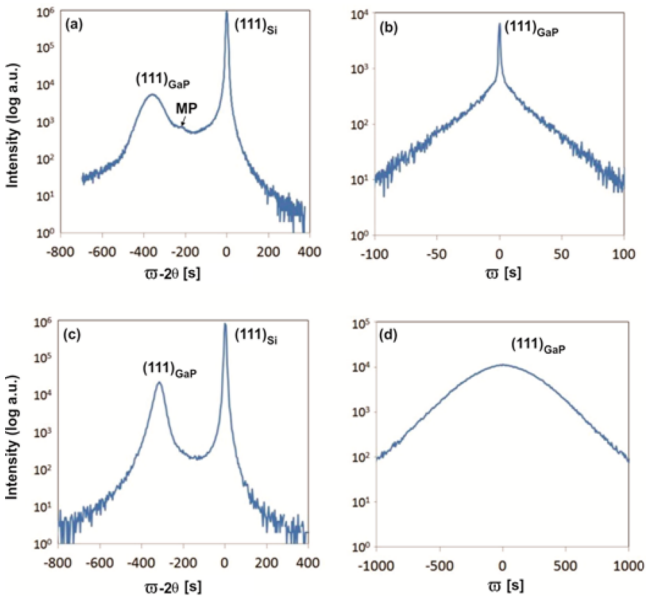

Figure 4. (a, b) $\omega-2\theta$ and ω rocking curves taken around the {111} diffraction peak of 200 nm GaP films grown on the no-miscut substrate, (c, d) corresponding curves for the 800 nm films on the miscut substrates. MP in a denotes a minor peak.

{111} reflection associated with single-crystal GaP. This is a clear indication that the films have grown epitaxially on both the no-miscut and miscut {111} Si substrates.

The position of the {111} diffraction peak of GaP films relative to that of the Si substrate can be used to estimate the strained state, which changes with the extent of the elastic coherency breakdown during the epitaxial growth. For 200 nm GaP films grown on the no-miscut substrate (cf. Figure 4a), the difference, $\Delta\theta_{S-L}$ (= $\theta_S - \theta_L$), between the {111} diffraction peaks of Si (θ_S) and GaP (θ_L)is found from the recorded spectrum to be 0.09944°. The magnitude of this angle difference can be used to estimate the relative difference between the *d*-spacing d_{111}^{GaP} and d_{111}^{Si} of the GaP film and Si substrate respectively, using the formula; $((d_{111}^{GaP} - d_{111}^{Si})/d_{111}^{Si}) = \{(\sin\theta_s/(\sin(\theta_s - \Delta\theta_{S-L})) - 1\} \times 100$, which is calculated to be 0.73%. Because the d_{111}^{Si} is 0.3135 nm, the d_{111}^{GaP}becomes 0.3158 nm, which is very close to the d_{111}^{GaP} (= 0.3157 nm) of a fully strained GaP film. It means that the GaP film deposited on the no-miscut substrate is almost fully strained without any elastic relaxation. In addition to the presence of the major peak, there is another minor peak (marked by a symbol, MP in Figure 4) that corresponds to$\Delta\theta_{S-L}$ = 0.0578°. The d_{111}^{GaP} for this minor peak is found to be 0.3148 nm, which is basically the same as the value of fully relaxed GaP (= 0.3147 nm). Thus, the GaP films grown on the no-miscut substrate contain both fully strained and fully relaxed regions.

The d_{111}^{GaP} of 800 nm GaP films grown on the miscut substrate, on the other hand, was 0.3155 nm. Because the *d*-spacing of bulk {111} GaP is 0.3147 nm, a fully strained GaP film grown on {111} Si should be 0.3157 nm. Therefore, the GaP films deposited on the miscut Si are almost fully strained.

The different strained states observed above can be further seen in detail as a difference in the ω rocking curves between the GaP films grown on the no-miscut substrate and those on the miscut substrate (compare Figures 4b, d). In Figure 4b, the no-miscut sample exhibits a narrow peak with the full width at half-maximum (FWHM) of approximately 0.005°, lying on top of a broad peak having the FWHM of 0.0989°. The narrow and broad peaks strongly indicate that there are two distinct regions, i.e., high- and low-crystal-quality regions. These two regions can be described in terms of the dislocation density, ρ, using the following formula[20]

$$\rho = \frac{(\mathrm{FWHM})^2}{4.35 \cdot |\mathbf{b}|^2}$$

where **b** (= $(a/2)\langle 110\rangle$) is the Burgers vector of a dislocation in GaP. Then the dislocation density in the high crystal-quality region is estimated to be ~1×10^6 cm^{-2}, whereas that in the low crystal-quality region is on the order of 2×10^6 to 1×10^9 cm^{-2}. The lateral coherence length, *L*, of these two regions can also be obtained from the ω-scan peak using[21]

$$L = \frac{0.9\lambda}{(\mathrm{FWHM})\sin\theta}$$

where λ (=1.54056 Å) is the wavelength of CuKα and θ (= 14.29°) the diffraction angle of {111} GaP. The coherence length of the high crystal-quality region for the films grown on the no-miscut substrate becomes ~6 μm, which is surprisingly 10 times larger than that (200−700 nm) of the low-crystal-quality region.

The film grown on the miscut substrate, on the other hand, gave only one broad peak in the ω-scan with the FWHM of 0.1528° (see Figure 4d). The broad peak indicates that the film is uniformly strained. The lateral coherence length of this film was found to be ~200 nm and the threading dislocation density was ~1×10^9 cm^{-2}. It is interesting to note that the magnitude of the dislocation density is comparable to that of the low-crystal-quality region in the films grown on the no-miscut substrates.

The presence of the superimposed sharp and broad peaks in the ω scan seen in the film grown on the no-miscut substrate is intriguing. It is important to note that the superimposed sharp/broad peaks does persist with increasing film thickness up to ~600 nm and thus they appear to be independent of the film thickness. This mechanism behind this result was investigated by TEM analysis of the film microstructure and will be discussed further in Section 3.8.

3.6. Cross-Section TEM and EDX Analysis. *3.6.1. GaP Films Grown on the Miscut Substrates.* Figure 5 is a (a) bright- (BF) and (b) dark-field (DF) TEM pair, showing the cross-section of the 800 nm thick GaP film grown on the miscut substrate. Threading dislocations run vertical to the interface and apparently originate from the interface. In addition, there are particles (marked as P) lying at the interface (cf. Figure 5a). The shape of the particles resembles the cross section of an onion, in which dislocations surround the particles. This morphology clearly indicates that a lattice mismatch exists between the GaP matrix and the particle. Based on the number of the threading dislocations, we estimate the number density to be ~2 × 10^{10} cm^{-2}, which is 1 order of magnitude higher than that (~2 × 10^{9} cm^{-2}) estimated by HRXRD. Since the distribution of the threading dislocations may not be uniform, it is possible that the dislocation density in the TEM cross sectional area (Figure 5), which samples only the small localized area, may exceed the average dislocation density of the film.

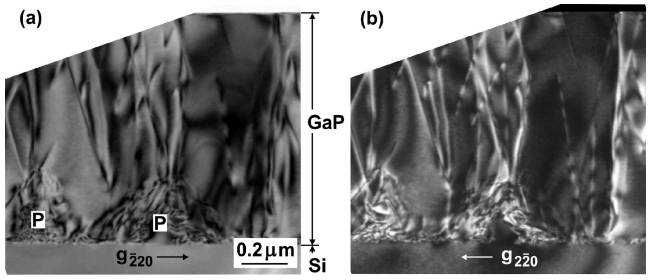

Figure 5. (a) BF and (b) DF pair of cross-sectional TEM images for a 800 nm thick GaP film grown on the miscut Si substrate, taken under the {220} two-beam conditions. The presence of particles at the GaP/Si interface is indicated by a symbol, P.

To further understand the nature of these particles, we applied the HAADF imaging technique, which was found to be useful in identifying the type of inclusions in the GaP films. Intensity variations seen in HAADF images can provide useful information on the type of particles seen in Figure 5. In general, in the HAADF imaging, increasing intensity (brightness) indicates increasing atomic number.

Figure 6 is the HAADF image together with EDX elemental line scans taken from the cross-sectional sample of a 1 μm GaP film grown on the miscut Si substrate. In the HAADF image (cf. Figure 6a), there are several darker areas (marked with white triangles) inside the cross-section of the GaP film which indicates the presence of lower Z atomic elements or voids. In this case, these darker areas are likely nanoclusters consisting of a low Z atomic element (lower than Ga and P atoms), which are hypothesized to be Si particles. One of these clusters was further analyzed using an EDX line scan along the line $X-Y$ shown in Figure 6a. Figure 6b is the $X-Y$ line scan taken for Si, P, and Ga peaks. It is clear from the scan that the dark objects are indeed Si particles. These Si particles appear to be

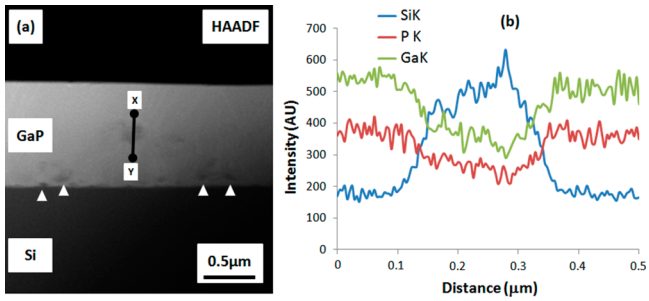

Figure 6. (a) HAADF image of the cross-section sample of a 1 μm thick GaP film grown on the miscut Si substrate. The EDX line scan across the X-Y line in a is plotted in (b) for Si Kα, P Kα, and Ga Kα lines.

distributed more at the GaP/Si interface, but to a lesser extent are scattered throughout the film thickness. A further TEM examination indicated that these Si particles are randomly oriented crystallographically inside the GaP film matrix. Nevertheless, this observation explains the large amount of Si that was detected by EDX attached to SEM. Figure 7 shows (a) the HAADF image and the corresponding EDX elemental maps taken from (b) Ga, (c) P, and (d) Si signals. It can be easily recognized from the Si elemental map (Figure 7d) that two particles, marked with white arrows in the HAADF image of Figure 7a, are Si.

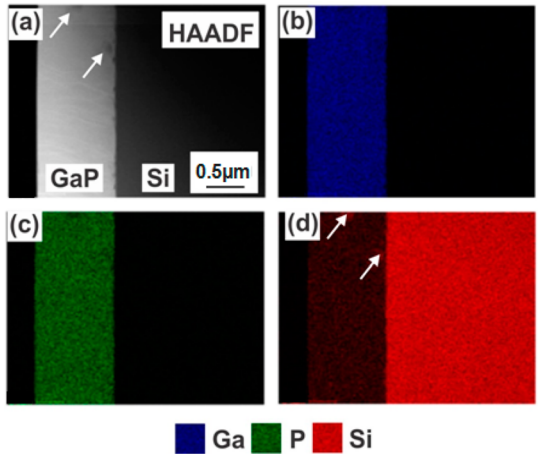

Figure 7. (a) HAADF image showing the cross section of a 1 μm thick GaP film grown on the miscut Si substrate. The corresponding EDX elemental maps are seen for (b) Ga, (c) P, and (d) Si atoms. Co-deposited Si particles are highlighted with white arrows.

In addition to the Si particles, a few Sn particles were observed in this film. Figure 8a is a HAADF image showing one round Sn particle lying near the GaP/Si interface. The corresponding magnified image together with an EDX Sn map is shown in images b and c in Figure 8. Although these Sn particles were present in this film, the Si particles were more dominant inclusions.

3.6.2. GaP Films Grown on the No-Miscut Substrate. The cross-section sample a 50 nm GaP film deposited on the no-miscut substrates revealed a surprising result different from that grown on the miscut substrates. First of all, the cross-sectional sample of the GaP films contained few threading dislocations, consistent with the morphology seen in Figure 1b. Figure 9 is a HAADF image showing the cross section of the GaP film

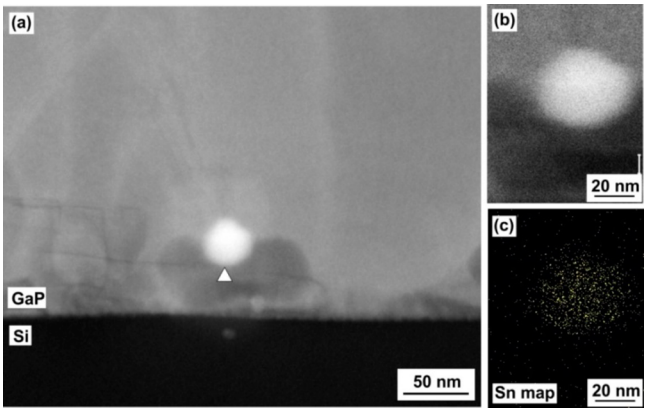

Figure 8. (a) HAADF image of a round particle (marked with a white triangle) in the 1 μm thick GaP film grown on the miscut substrate. (b) Magnified image of the HAADF image is compared with (c) the corresponding EDX Sn map.

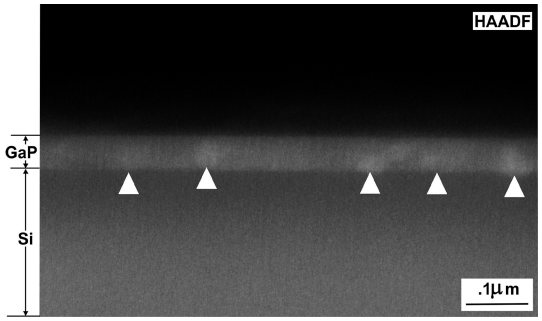

Figure 9. Sn particles seen in the cross-section sample of a 50 nm thick GaP film, which was grown on the no-miscut substrate. Sn particles marked with white triangles are seen as a bright object in the HAADF image.

grown on the no-miscut substrate. Contrary to the image seen in Figure 6a, the inclusion images display above-background intensity (see Figure 9). Furthermore, most of these images lie at the GaP/Si interface. These particles were analyzed using an EDX line scan, which is taken along the X-Y line drawn in Figure 10a. It is clear from the Sn L peak (Figure 10d) that these particles correspond to Sn particles. The size and number density of these Sn particles were found to be 40−70 nm and 5 × 10^2 cm^{-2}, respectively. From this data, we estimate that the Sn particles occupy as much as 10% of the GaP film area. The extent of this coverage is quite significant and thus it may alter the film property, as will be discussed in Section 3.8.

Si inclusions are also undoubtedly present in this film. The presence of Sn particles, however, was dominant, and thus images of Si particles were not captured easily in the HAADF images.

3.6.3. Difference in Inclusions between the Two Types of Substrates. Because Sn is used as the bath solvent, it is conceivable that Sn could be incorporated into the GaP films. It is, however, not clear why a large number of Sn particles were present on the no-miscut substrate but not on the miscut surface. One possible cause is due to the slow growth rate of GaP films on the no-miscut surface. The no-miscut surface does not contain enough steps to initiate the GaP growth, which then requires two- or three-dimensional nucleations. It is possible that the growth rate may be even slower at the beginning stages of nucleation and growth. This initial slow nucleation process allows Sn to be incorporated readily into the GaP film. Consequently, more Sn particles are seen in the GaP film. This result strongly suggests that Sn incorporation may depend on the growth rate of the GaP film, which, in turn, is affected by the initial surface condition of the substrate.

For the Si inclusions, more Si particles were found to be incorporated into the GaP film grown on the miscut surface. These particles appear to be incorporated close to the GaP/Si

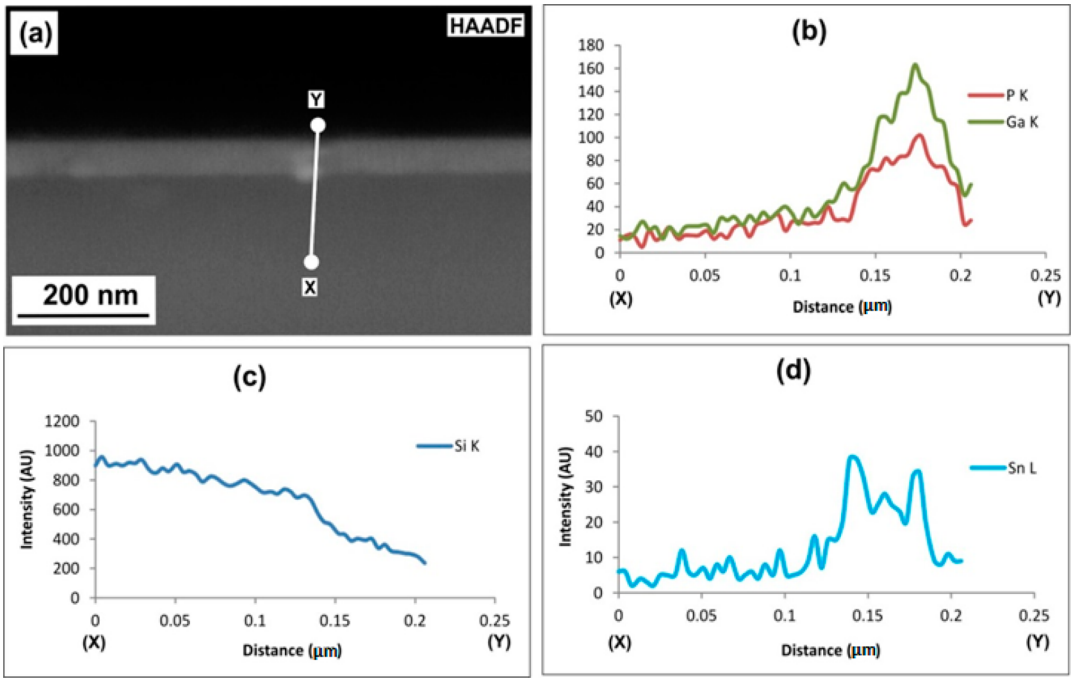

Figure 10. (a) HAADF image showing the cross section of a 50 nm GaP film grown on the no-miscut substrate. The EDX line scan was taken across the X−Y line in a for (b) P Kα/Ga Kα, (c) Si Kα, and (d) Sn Lα lines.

interface (see Figures 5 and 6a). Because the LPE solution is saturated with Si, the GaP deposition and Si incorporation might be a competitive process, despite that fact that the solubility of Si is ~80 times higher than that of GaP in the Sn solution at the growth temperature. In the initial stages of nucleation and growth, Si incorporation (or deposition) may be easier on the miscut surface than on the no-miscut surface, because the miscut surface already contains a number of steps, where Si, Ga, and P atoms can deposit. Si deposition on Si substrate should be energetically more favorable than GaP deposition. Thus, we see more Si particles on the miscut interface.

3.7. Residue Analysis. The surface residue left after Br-methanol etching of the 200 nm thick GaP film grown on the no-miscut Si was studied. An SEM micrograph revealed that the residue left on the substrate consisted of small particles (see Figure 11). The residue was placed on a carbon-coated Cu backed carbon support film, respectively. It has been demonstrated that an analysis of the residue is a convenient way of determining the type of impurity atoms incorporated in LPE GaP films. The large Sn peaks indeed are consistent with the interfacial Sn particles observed in the cross-section TEM.

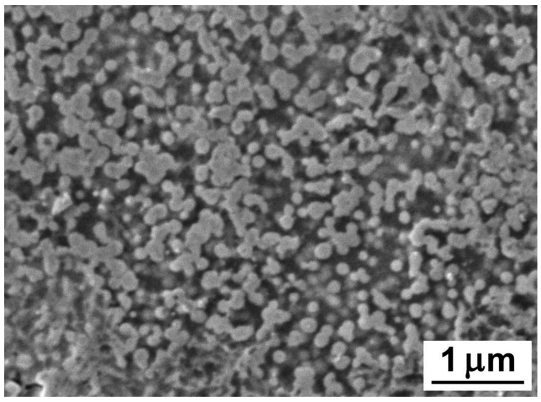

Figure 11. SEM of a surface residue left on the no-miscut Si substrate after etching the 200 nm thick GaP film in a Br-methanol solution.

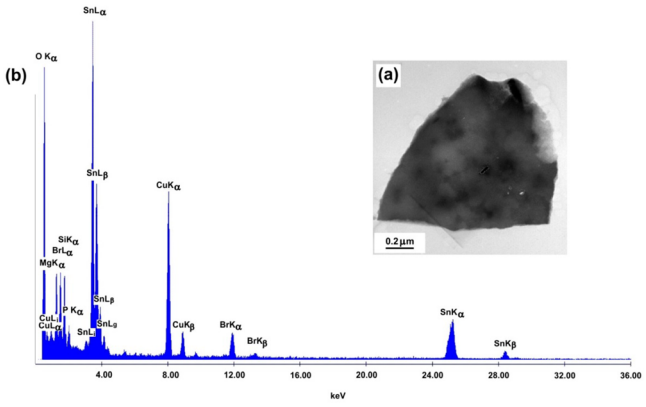

Figure 12. (a) Image of a typical residue piece collected on a carbon-coated copper TEM grid and (b) its EDX spectrum.

TEM grid and examined by TEM. Figure 12 shows (a) one typical particle on the copper grid and (b) its EDX spectrum. As expected from the cross-section TEM work, large peaks of Sn appeared in the spectrum. In addition to the Sn peaks, there are other peaks, such as Si and Mg, associated with the observed inclusions. We also note the peak from Br, which was the part of the Br-methanol etchant. The Cu peaks as well as the oxygen peaks originate from the grid and the Formbar-

3.8. Mechanism of the Formation of the Microstructure Consisting of Strained and Strain-Free Regions. It has been shown from the ω rocking curve that the 200 nm GaP film grown on the no-miscut substrate exhibits a unique rocking curve consisting of a superposition of sharp and broad peaks (see Figure 4b). We interpreted that there are two distinct regions that consist of high and low crystal-quality regions. Hereafter, for the sake of discussion, these two regions are referred as strain-free (high crystal quality) and strained (low crystal quality) regions, which correspond to sharp and broad peaks, respectively. It was found that this microstructural trend persists with increasing film thickness up to 600 nm. This trend, therefore, is independent of film thickness, thus ruling out the possibility that the strain-free region forms on a top layer along the film thickness direction as a result of the rearrangement/annihilation of threading dislocations. Consequently, the strained and strain-free regions must be distributed over the film plane rather than along the film thickness direction. A key answer to a question as to why this phenomenon occurred only in the GaP films grown on the no-miscut substrate must lie in the fact that a number (5×10^2 cm^{-2}) of large (40–70 nm) Sn particles were present in the GaP film.

On the basis of the above observations, we propose a model that explains why strained and strain-free regions form in the GaP films grown only on the no-miscut surface. As already noted in the TEM analysis, the presence of interfacial Sn particles must play a key role in creating the type of microstructure observed in the GaP film. Figure 13 is a

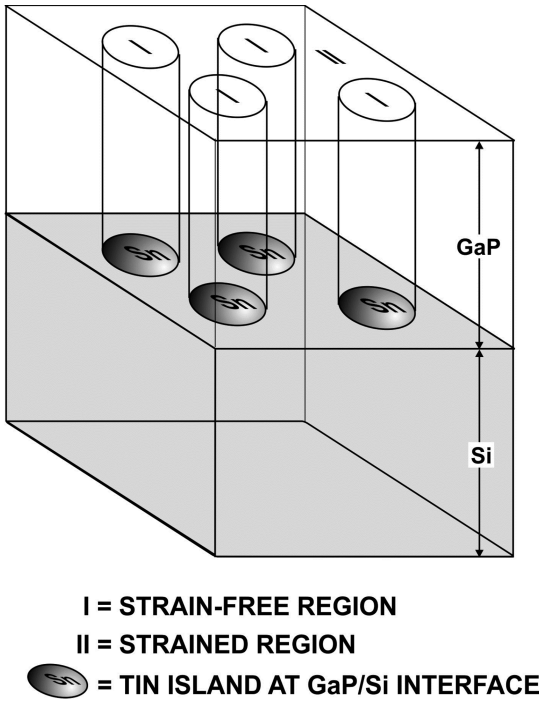

Figure 13. Schematic diagram showing how strain-free, I, and strained, II, regions are generated in a GaP film as a result of the presence of Sn islands adsorbed on the GaP/Si interface.

schematic view showing how two regions having two different strain states are generated during LPE growth. Consider the growth of a GaP film on a surface covered with a number of Sn islands. Phenomenologically speaking, the areas of the GaP film grown over the Sn islands are not affected by the coherency strain from the substrate and thus are strain-free. The areas of the GaP grown outside the Sn islands, on the other hand, is in direct contact to the substrate and thus becomes strained coherently or semicoherently. This results in forming strain-free (marked as I) and strained (marked as II) regions in the GaP film. It should be noted that the Sn is in a liquid state during the LPE growth. Thus, the solid Sn particles seen in the cross-section TEM sample were liquid during the GaP growth. It can be envisioned that GaP may not nucleate or grow directly over the liquid Sn but grow from the strained region toward the Sn islands in such a way to cover over them. According to the present model, therefore, the formation of this type of microstructure depends only on the distribution of the Sn islands.

To the best of the authors' knowledge, there are no other publications that report a similar observation. However, an observation was made by Darhuber et al.,[22] who previously reported a ω scan peak exhibiting a sharp peak superimposed with a broad peak and attributed the peak due to lateral ordering in vertically aligned quantum dots.

4. CONCLUSION

It has been demonstrated that uniform epitaxial GaP layers can be grown by liquid phase epitaxy on {111} Si substrates from a tin-based solvent bath containing an appropriate reducing agent and surfactant. An elemental mapping of the cross-section of the GaP/Si samples, however, has revealed that both Si and Sn are incorporated as particles. The distribution of these particles was highly dependent on the orientation of the Si substrate. Particularly, in the case of the exactly oriented {111} Si substrate, a number ($\sim 5 \times 10^2$ cm^{-2}) of large (40−70 nm) Sn particles were preferentially codeposited at the GaP/Si interface. The incorporation of these Sn particles resulted in a duplex microstructure consisting of strained and strain-free regions in the GaP films.

On the basis of the above observation, we propose a mechanism as to how such a microstructure forms in the GaP film containing interfacial Sn particles; the part of the GaP films lying directly above the Sn particles is completely noncoherent to the underlying Sn/Si substrate and thus becomes strain-free (unstrained). According to this mechanism, the formation of the duplex structure requires only the interfacial Sn particles, but not those incorporated in any other locations in the film. A concept of this mechanism may be useful in tailoring the fabrication of a new type of microstructure in LPE films that take advantage of the strain-free high-crystal-quality regions of the resulting GaP film to produce subsequent films with reduced threading dislocation densities. Finally, one novel application of the present GaP films is to use them as a seed layer for growing further GaP layers using different solvents, which might duplicate the unique microstructure of the underlying GaP layer.

AUTHOR INFORMATION

Corresponding Authors

*E-mail: rhuang@udel.edu.
*E-mail: opila@udel.edu.

Present Addresses

‡S.R.H. is currently at 950 L'Enfant Plaza, Washington, DC 20024.
⊥X.L. is currently at Applied Materials Inc., Santa Clara, CA 95130.
#A.B is currently at School of Photovoltaics, University of New South Wales, Sydney, NSW, Australia 2052.

Author Contributions

The manuscript was written through contributions of all authors. All authors have given approval to the final version of the manuscript.

Funding

This research was, in part, funded by the U.S. Government Defense Advanced Research Projects Agency under Agreement HR0011−0709−0005. The TEM work was conducted at the University of Limerick under framework of the INSPIRE program, funded by Irish government's Program for Research in Third Level Institutes, Cycle 4, National Development Plan 2007−2013.

Notes

The authors declare no competing financial interest.

ABBREVIATIONS

GaP, gallium phosphide
LPE, liquid phase epitaxy
EDX, energy-dispersive X-ray
HAADF, high-angle annular dark field
HRXRD, high-resolution X-ray diffraction
TEM, transmission electron microscopy

REFERENCES

(1) Astles, M. G. *Liquid-Phase Epitaxial Growth of III-V Compound Semiconductor Materials and their Device Applications*; Adam Hilger: New York, 1990; pp 2−3.
(2) Katoda, T.; Kishi, M. Heteroepitaxial Growth of Gallium Phosphide on Silicon. *J. Electron. Mater.* **1980**, *9*, 783−796.
(3) Sugo, M. Growth of Antiphase-Domain-Free GaP on Si by Organometallic Vapor Phase Epitaxy. *J. Cryst. Growth* **1988**, *88*, 229−235.
(4) Narayanan, V.; Sukidi, C.; Hu, C.; Dietz, N.; Bachmann, K. J.; Mahajan, S.; Shingubara, S. Growth of Gallium Phosphide Layers by Chemical Beam Epitaxy on Oxide Patterned (001)Silicon Substrates. *Mater. Sci. Eng., B* **1998**, *54*, 207−209.
(5) Grassman, T.; Brenner, M.; Rajagopalan, S.; Unocic, R.; Dehoff, R.; Mills, M.; Fraser, H.; Ringel, S. Control and Elimination of Nucleation-Related Defects in GaP/Si(001) Heteroepitaxy. *Appl. Phys. Lett.* **2009**, *94*, 232106.
(6) Igarashi, O. Two-Stage Epitaxial Growth of GaP on Si. *Jpn. J. Appl. Phys.* **1977**, *16*, 1863−1864.
(7) Jussila, H.; Nagarajan, S.; Mattila, P.; Riikonen, J.; Huhtio, T.; Sopanen, M.; Lipsanen, H. Growth and Characterization of GaP Layers on Silicon Substrates by Metal-organic Vapour Phase Epitaxy. Phys. *Status Solidi C* **2012**, *9*, 1607−1609.
(8) Grassman, T. J.; Carlin, J. A.; Galiana, B.; Yang, F.; Mills, M. J.; Ringel, S. A. MOCVD-Grown GaP/Si Subcells for Integrated III-V/Si Multijunction Photovoltaics. *IEEE J. Photovolt.* **2014**, *14*, 972−980.
(9) Beneking, H.; Roehle, H.; Mischel, P.; Schul, G. Growth and Properties of GaP Liquid Phase Epitaxial Layers on Si Substrates. *Proceedings of the Sixth International Symposium on Gallium Arsenide and Related Compounds*; CRC Press: New York, 1977; pp 51−57.
(10) Rosztoczy, F.; Stein, W. The Growth of Ge-GaAs and GaP-Si Heterojunctions by Liquid Phase Epitaxy. *J. Electrochem. Soc.* **1972**, *119*, 1119−1121.
(11) Scheel, H. J. Introduction to Liquid Phase Epitaxy. *In Liquid Phase Epitaxy of Electronic, Optical and Optoelectronic Materials*;

Capper, P.; Mauk, M., Eds.; John Wiley & Sons: New York, 2007; pp 1−17.
(12) Saidov, M.; Saidov, A.; Dadamukhamedov, S. Influence of A^3B^5 Compounds on the Solubility of Silicon in Tin. *Dokl. Akad. Nauk UzSSR* **1976**, *8*, 24−25.
(13) Sugihara, S.; Okazaki, K.; Suganuma, K. Wetting of Silicon Single Crystal by Silver and Tin, and Their Interfaces. *J. Mater. Sci.* **1993**, *28*, 2455−2458.
(14) Horn-von Hoegen, M.; Meyer zu Heringdorf, F. J.; Kammler, M.; Schaeffer, C.; Reinking, D.; Hofmann, K. R. Bi Surfactant Mediated Epitaxy of Ge on Si(111). *Thin Solid Films* **1999**, *343−344*, 579−582.
(15) Mauk, M. G.; Curran, J. P. Electro-epitaxial Lateral Overgrowth of Silicon from Liquid-Metal Solutions. *J. Cryst. Growth* **2001**, *225*, 348−353.
(16) Zhong, L.; Takeda, R.; Izunome, K.; Matsushita, Y.; Aiba, Y.; Matsushita, J.; Yoshikawa, J.; Hayashi, K.; Shirai, H.; Saito, H. Surface Modification of Silicon (111) by Annealing at High Temperature in Hydrogen. *Appl. Phys. Lett.* **1996**, *68*, 2349−2351.
(17) Nakahara, S.; Chu, S. N. G.; Long, J. A.; Riggs, V. G.; Johnston, W. D., Jr. A Transmission Electron Microscopy Study of Iron Phosphide Precipitates in InP Crystals. *J. Cryst. Growth* **1985**, *72*, 693−698.
(18) Heimbrook, L. A. K.; Moyers, W.; Nakahara, S. New Technique for Analyzing Small Inclusions Using Transmission Electron Microscopy and Laser Ablation Microprobe Mass. *Mater. Lett.* **1990**, *9*, 384−388.
(19) Briggs, M. S. D. *Practical Surface Analysis: By Auger and X-Ray Photoelectron Spectroscopy*, 2nd ed.; John Wiley & Sons: New York, 1993; Vol. *2*.
(20) Dunn, C. G.; Kogh, E. F. Comparison of Dislocation Densities of Primary and Secondary Recrystallization Grains of Si-Fe. *Acta Metall.* **1957**, *5*, 548−554.
(21) Warren, B. E. *X-ray Diffraction*, 1st ed.; Dover Publications: New York, 1990; pp 251−254.
(22) Darhuber, A. A.; Holy, V.; Stangl, J.; Bauer, G.; Krost, A.; Heinrichsdorff, F.; Grundmann, M.; Bimberg, D.; Ustinov, V. M.; Kop'ev, P. S.; Kosogov, A. O.; Werner, P. Lateral and Vertical Ordering in Multilayered Self-Organized InGaAs Quantum Dots Studied by High Resolution X-ray Diffraction. *Appl. Phys. Lett.* **1997**, *70*, 955−957.